

Thesis for the Degree of Master of Science

MURO:
Mangpo high school
Unmanned Remote Observatory

Hyunjong Kim

School of Space Research
Graduate School
Kyung Hee University
Seoul, Korea

February, 2019

MURO:
Mangpo high school
Unmanned Remote Observatory

Hyunjong Kim

School of Space Research
Graduate School
Kyung Hee University
Seoul, Korea

February, 2019

MURO:
Mangpo high school
Unmanned Remote Observatory

by
Hyunjong Kim

Advised by
Dr. Soojong Pak

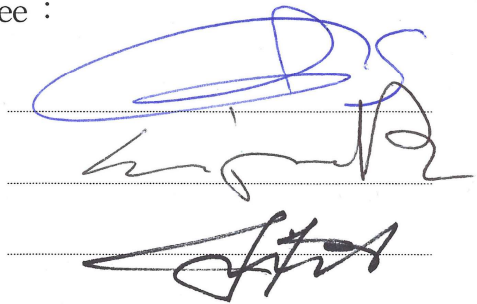
Submitted to the School of Space Research
and the Faculty of the Graduate School of
Kyung Hee University in partial fulfillment
of the requirements for degree of
Master of Science

Dissertation Committee :

Prof. Myungshin Im(Chairman), Ph. D

Prof. Soojong Pak, Ph. D

Prof. Ho Jin, Ph. D

Three handwritten signatures are displayed on horizontal lines. The top signature is in blue ink and is highly stylized. The middle signature is in black ink and is also stylized. The bottom signature is in black ink and is more legible, appearing to read 'Ho Jin'.

<ABSTRACT>

MURO:

Mangpo high school Unmanned Remote Observatory

by Hyunjong Kim

Master of Science in School of Space Research

Graduate School of Kyung Hee University

Advised by Dr. Soojong Pak

We introduce the observational characteristics of the Mangpo high school Unmanned Remote Observatory(MURO) which was installed at the Yangpyeong, Gyeonggi-do, Republic of Korea in 2015 January. The remote 0.25m telescope with a pixel scale of 1.485 arcsec($9\mu\text{m}$) in $4K \times 4K$ CCD camera provides $1.69^\circ \times 1.69^\circ$ wide field of view(FOV). It is equipped with the $UBVR_cI_c$ filters, narrow band(5nm bandwidth) filters and $LRGB$ imaging filters. We examine properties photometric reliability of MURO such as bias level, dark current, standardization, and characteristics of system. The data reduction was performed by observing standard stars and NGC 869 / 884 open clusters with AstroImageJ(AIJ). MURO provides a good images that the limiting magnitude of $B = 18.308\text{mag}$, $V = 18.547\text{mag}$, $R = 19.096\text{mag}$, $I = 16.887\text{mag}$ at $10\text{-}\sigma$ with 120 sec exposure time. It can be available to serious astronomical research and citizen astronomy projects; making and analyzing new observations, visually classifying features in images and light curves by high school and college students or public school teachers, as well as professional astronomers.

Key words

instrumentation: photometers, techniques: photometric

<국문 초록>

MURO: Mangpo high school Unmanned Remote Observatory

by Hyunjong Kim
Master of Science in School of Space Research
Graduate School of Kyung Hee University
Advised by Dr. Soojong Pak

이 연구에서는 2015년 1월, 경기도 양평에 설치된 망포 고등학교의 무인 원격 천문대(MURO)의 천문학적 특징을 소개한다. 원격으로 제어되는 0.25m 망원경은 1.485 arcsec ($9\mu\text{m}$)의 픽셀 스케일을 가진 $4K \times 4K$ CCD 카메라를 장착하여 $1.69^\circ \times 1.69^\circ$ 의 넓은 화각(FOV)을 제공한다. 이 시스템에는 $UBVR_cI_c$ 측광 필터, 협대역(5nm 대역폭) 필터 및 $LRGB$ 이미징 필터가 장착되어 있다. 여기에서는 MURO의 바이어스 레벨, 암전류, 등급 표준화 등의 측광학적 안정성과 관측 시스템의 특징을 점검하고 기술하였다. 데이터 처리는 표준성과 NGC 869 / 884 산개성단을 관측하여 AstroImageJ(AIJ)로 수행하였다. MURO는 노출 시간 120초와 신호 대 잡음비 $10-\sigma$ 에서 B 등급 = 18.308mag, V 등급 = 18.547mag, R 등급 = 19.096mag, I 등급 = 16.887mag의 우수한 성능을 제공한다. 이 시스템은 새로운 천체를 관측하고 분석하거나 천체의 광도 변화 특징을 분류하는 등의 수준 높은 천문학적 연구와 시민 천문학 프로젝트에 활용될 수 있으며, 전문적인 천문학자뿐만 아니라 고등학생과 대학생, 교사 등을 위한 교육적 프로그램에도 활용이 가능하다.

키 워드

관측기기: 측광 장치, 관측 기술: 측광학

< Contents >

1. Introduction	1
2. Overview of MURO	3
2.1. Observatory Control Package(OCP)	5
2.2. Telescope Control Package(TCP)	11
2.3. Data Taking Package(DTP)	13
3. Data Reduction	20
4. Standardization Results	23
4.1. Standard Star Observation	23
4.2. NGC 869 / 884 Observation	27
5. Summary	32

< List of Figures >

1. The architecture diagram of MURO.	3
2. The exterior appearance of MURO.	4
3. Equip the eight of 2kg weight ballast.	6
4. Four of heat sensor camera default position.	8
5. Devices that provide atmosphere and weather information.	10
6. CCA-250 telescope system in MURO.	14
7. The QE of Truesense KAF-16803 sensor.	18
8. The bias, dark, and flat field frames taken with Maxim DL.	22
9. Slope of function for BVRI filters.	25
10. Photometric target region of NGC 869 / 884.	28
11. The limiting magnitudes of MURO.	30
12. The color – magnitude diagram result.	31

< List of Tables >

1. Sensor specifications of the Auto-guide System.	12
2. Characteristics of the CCA-250.	15
3. Sensor specifications of the FLI PL 16803 and performance.	17
4. Filter wavelengths and widths.	19
5. Photometric calibration parameters from standard star data.	26
6. Photometric calibration parameters from NGC 869 / 884 data.	30

1. Introduction

Recent developments of large format and wide-field imaging instruments for specific purpose are qualified to manufacture and execution. And the need for small wide-field telescopes are becoming important because of their convenient accessibility, fast photometry and ease of fabrication and installation. Small telescope has many advantages in order to astronomical research. It is easy to access global network of telescope, e.g., the LCOGT(Brown et al. 2013), Citizen Science(Marshall et al. 2015) and to studies of NEOs(Tarady et al. 2014) or small planets, e.g., the MINERVA(Wittenmyer et al. 2015), enable fast photometry and high photometry accuracy(Kanbach et al. 2014; Grauer, 2008), also can possible automatic and remote observations, e.g., the U-SmART(Gupta et al. 2015), pt5m(Hardy et al. 2015), Liverpool Telescope(Steele et al. 2004). Most of the observatories are operated robotic system, but it often breaks down with electronic program control parts than remote type.

Small wide-field telescopes designed for these special purposes are expensive, time-consuming, and require specialized research personnel. That can sharply reduce operation costs as they require much less staff interaction. So many commercial instruments are being utilized in astronomical science research with remote or robotic type(e.g. Zerbi et al. 2001; French et al. 2004; Tsapras et al. 2009; Gillon et al. 2011; Gorbovskoy et al. 2013; Snellen et al. 2012; Schmitt et al. 2014; Strolger et al. 2014). Also, the chance of small telescope taking parts in scientific research is increasing especially in fields of transient objects and variable stars. A large amount of the photometric data for either supernovae or variable stars are available with commercial telescope and science cameras(Park et al. 2016), detection of an impact flash on the moon(Kim et al. 2015), intensive monitoring survey of nearby galaxies, e.g., the LSGT(Im et al. 2015; Choi et al. 2017), jupiter's atmosphere zonal winds study(Barrado-Izagirre et al.

2013). However, there are limitations in the installation method or it needs an optimize device combinations to avoid the performance of the equipment is degraded or unreliable. And commercial instruments must be tested for overall performance, as it is difficult to fully trust the manufacturer's specifications.

Therefore, we carry out this research to study the possibility of astronomical science using commercial instruments of The MURO. It completed in order to perform a variety of science that utilizes with a small wide-field remote telescope in 2015 January. Here we describe MURO's aims and the hardware and software systems that we have built to meet them. The remainder of the paper is organized as follows. Section 2 gives a characteristic of telescope and describes the performance of MURO to study the possibility of astronomical science. Section 3 will show about how to do data reduction with AstroImageJ(AIJ). Section 4, we describe the standardization results of the photometric data compare with Landolt's observations data(Landolt, 2009) and NGC 869 / 884 open cluster data from SIMBAD astronomical database. Section 5 gives a brief summary and describes prospects for the future.

2. Overview of MURO

The MURO is consisted of three parts: The Observatory Control Package(OCP), the Telescope Control Package(TCP), the Data Taking Package(DTP). The architecture diagram of MURO is given in Figure 1, and exterior appearance of MURO shows Figure 2. Functioning of each component of system is fined below.

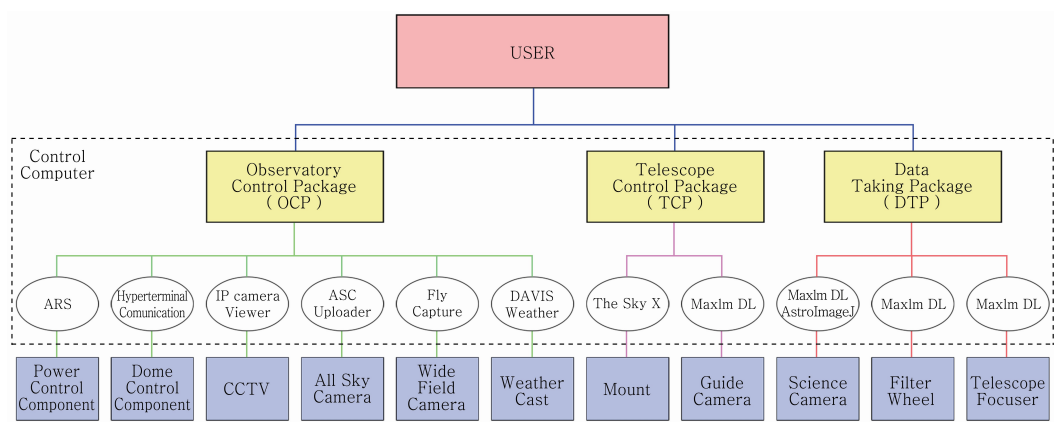


Figure 1. The architecture diagram of MURO.



Figure 2. The exterior appearance of MURO. (1) 2.1m fiberglass clamshell dome, (2) weather cast, (3) all sky camera.

2.1. Observatory Control Package(OCP)

MURO system was encosed 2.1m non-rotation fiberglass Astrohaven clamshell dome¹⁾, installed at Yangdong Elementary School Gosong Campus(longitude 37° 29 ' 11.0 " N, latitude 127° 42 ' 01.3 " E, altitude 200m) in Yangpyeong, Gyeonggi-do, KOREA, 2015. This site can observe a wide field of view, the atmospheric conditions are better than the Mangpo high school astro-laboratory in Suwon-si. It designed that component of north and south three shells. It is opened and closed respectively, switch gear system supports both automatic and manual operation. The switch gear system can be controlled through USB communication using a command line on Hyper-Terminal in Windows OS on the control computer. This dome is relatively lightweight and convenient advantage for rapid follow-up observations, no delay time without rotate dome. Also, we equip the eight of 2kg weight ballast at the lower portion of each shell to allow for smooth opening and closing to work better than the manufacturer's design. The Figure 3 shows the weight ballast at the lower portion of each shells.

1) <https://astrohaven.com>



Figure 3. Equip the eight of 2kg weight ballast of each shell to allow fully automatic opening and closing.

All of MURO components can be controlled by the two computers, standby computer and control computer. The power of the telescope can be controlled to remote tell-booter by ARS, driving is possible via control computer. Control computer can be directly adjust the components of MURO system, and it will always remain the power is turned off to protect from viruses or suffer damage by lightning and minimize the power loss. On the other hand standby computer will always remain the power is turned on for under surveillance with security camera. It can connect from Team Viewer program of Mangpo high school astro-laboratory, and it can be a turn on the control computer. After the power of control computer and telescope system turn on by remote tell-booter, all of the systems are controlled with control computer from Team Viewer program of Mangpo high school astro-laboratory.

Processes for using the MURO system is as follows.

1. turn-on the control computer by standby computer using remote wake-up method.
2. turn-on the power control component by remote tell-booter system.
3. connect control computer from Mangpo high school astro-laboratory with Team Viewer program.
4. connect dome control component and open the dome by Hyper-Terminal with control computer.
5. all of MURO system can be controlled by control computer.

And it ends in reverse order when all the observations are finished. This system can be used by anyone who has been approved by Mangpo high school astro-laboratory through a connection code of Team Viewer program.

Surveillance of the system is possible with four heat sensor cameras, that is always monitoring for inside of dome and the telescope. Security camera can overlook in real time for the north and south, east and west directions. Surveillance zone as possible to left/right 350 degrees and up/down 80 degrees. Figure 4 shows the default position of surveillance.

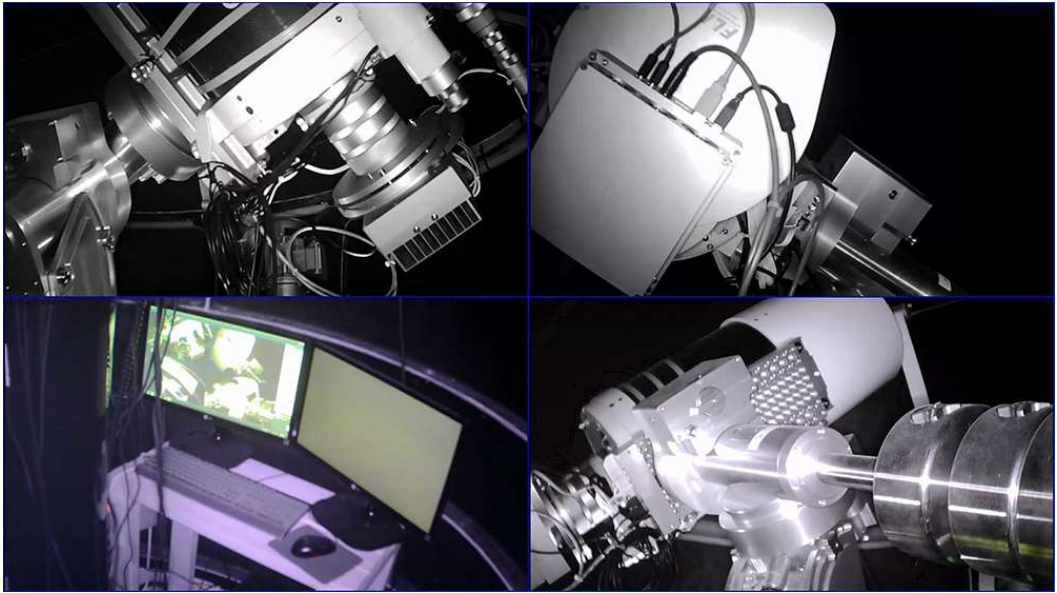


Figure 4. Four of heat sensor camera default position looking from each direction NSEW. Each camera look for CCD camera, telescope, mount, control computer and power supply.

The state of atmosphere and weather information can be found by DAVIS real-time weather cast and all sky camera and wide-field video camera. This equipment measures the cloudiness, temperature, humidity, wind strength and so on can determine the possibility of observations. In addition, all sky camera and wide-field video camera provide real-time visibility of cloud volume, satellite and aircraft paths. Therefore, it is possible to judge whether this affects the observation. Figure 5 shows the example image of all sky camera, wide-field video camera and weather cast system data. From March 2015 to February 2017 weather records, we anticipate 193 nights per year with at least 7.3 usable hours and median seeing of 3.56" .

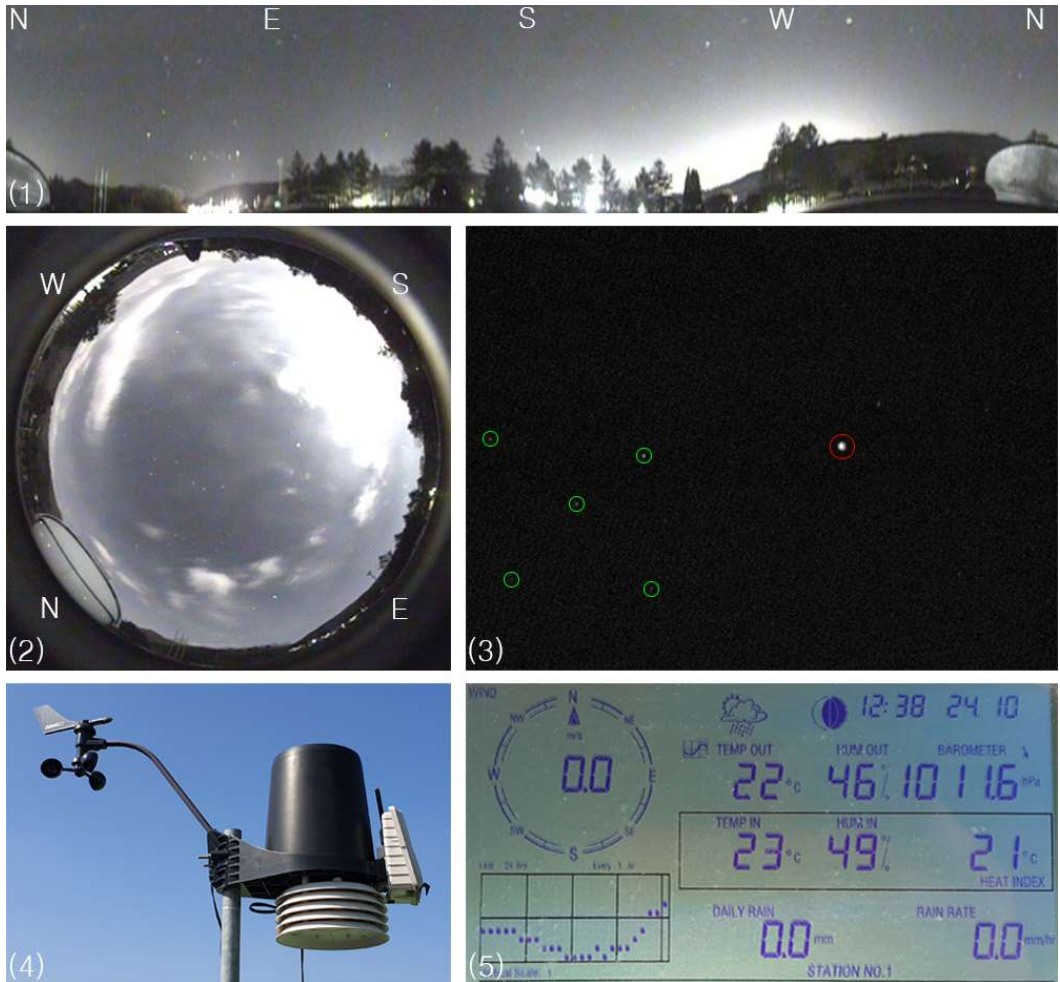


Figure 5. Devices that provide atmosphere and weather information. (1) Panoramic image of all sky camera taken at dark clear night. The bright areas of the western sky come from the lights of the city, (2) General image of all sky camera taken on the cloudy night of the moon, (3) The image taken with wide-field video camera(field of view is $15.9^{\circ} \times 11.8^{\circ}$. The green circles indicate the stars that constellation of Cygnus α , γ , δ , ϵ , η . And the red circle is an airplane, (4) The exterior appearance of DAVIS real-time weather cast, (5) The example data of weather cast.

2.2. Telescope Control Package(TCP)

Mount of MURO is the MEII equatorial model by Software Bisque, Inc. MEII is easier to use by eliminating the need to initialize the mount's position(through homing or synchronization) at start up or after power loss. Drive and control of the telescope's mount can possible with The Sky X and Maxim DL. All softwares are commercialized or freeware programs based on Windows OS, since it is difficult to access LINUX and IRAF package except for professional astronomers. Software based on Windows OS make easier to approachable students or amateur astronomers. After The Sky X connect telescope, the mount move to home position automatically. Provides improved pointing and tracking accuracy by continuously monitoring the position of the main gear, as opposed to encoder mounted directly to the motor's drive shaft. It can achieve maximum 7 arcseconds peak-to-peak periodic error from the manufacturer's specification²⁾. Now, however, it has improves by performing the T-pointing, estimated 3 arcseconds RMS.

Auto-guide system is not on the science camera but consists of a separate system. Guide telescope diameter is 60mm by Takahashi Seisakusho Ltd., and guide camera from Starlight Xpress Ltd. In Table 1, we tabulate the overall characteristics of the guide telescope and guide CCD sensor. For the focal ratio of f/5.9 of the 60mm guide telescope, the pixel scale on the sky can be calculated as

$$Horizontal\ pix = \frac{206265}{5.9 \times 60mm} \times 0.0082mm = 4.778''$$

$$Verical\ pix = \frac{206265}{5.9 \times 60mm} \times 0.0084mm = 4.849''$$

Therefore, the field of view of this guide system is $0.998^\circ \times 0.789^\circ$.

2) <https://optcorp.com>

Table 1
Sensor specifications of the Auto-guide System

Guide Telescope	
Diameter	60mm
Focal length	355mm
Focal ratio	f / 5.9
Optimal Field of View	44mm Image Circle
FOV with CCD	$0.998^{\circ} \times 0.789^{\circ}$
Guide CCD	
Sensor	ICX429AL Sony Exview interline
Pixels	752×580
Pixel Size	$8.2\mu\text{m} \times 8.4\mu\text{m}$
Sensor Size	$6.4\text{mm} \times 4.75\text{mm}$
Typical Dark Current	$< 0.1\text{e}^-/\text{pixel}/\text{sec}$ at 10°C
Readout Noise	$< 15\text{e}^-$ RMS
Quantum Efficiency	Maximum 65% at 650nm

^aThese data of specifications measured by manufacturer, Starlight Xpress Ltd.,

2.3. Data Taking Package(DTP)

We use a 0.25m telescope with an effective focal length of 1.25m(Corrected Cassegrain Astrograph, CCA-250, Takahashi Seisakusho Ltd.). It employs a corrected cassegrain optical system with a large three element correctors to produce a point spread function(PSF) size of $6 \sim 10 \mu\text{m}$ inside the diameter of 88mm on the focal plane³⁾. The instruments of DTP's elements are illustrated in the Figure 6, and we provide the overall characteristics of the CCA-250 in Table 2. Since the winter minimum temperature lowered to less than -18°C of local observatory installed, emplace additional heating band. It operates simultaneously with main power on, prevent to made glacial frost in astrograph. So maintain one degree higher in astrograph main mirror than ambient temperature by three computers controlled cooling fans and heating band. The CCD camera and the cooling system were put together by Finger Lakes Instrumentation, Inc. It is a 16803 Series camera system in their production line, full frame sensor operation up to 14MHz(16-bit), sensor cooling up to 55°C below ambient air cooled. The CCD chip on the camera is manufactured by the Truesense KAF-16803. The chip has an active area in an array of 4096×4096 pixels. Physical scale of each square pixel is $9 \mu\text{m}$, which gives the overall imaging area of $36.8 \times 36.8 \text{ mm}$. For the focal ratio of f/5 of the 0.25m telescope, the pixel scale on the sky can be calculated as

$$pix \ scale = \frac{206265}{5.0 \times 250mm} \times 0.009mm = 1.485''$$

Therefore, the field of view of this guide system is $1.69^{\circ} \times 1.69^{\circ}$.

3) <http://www.takahashijapan.com>

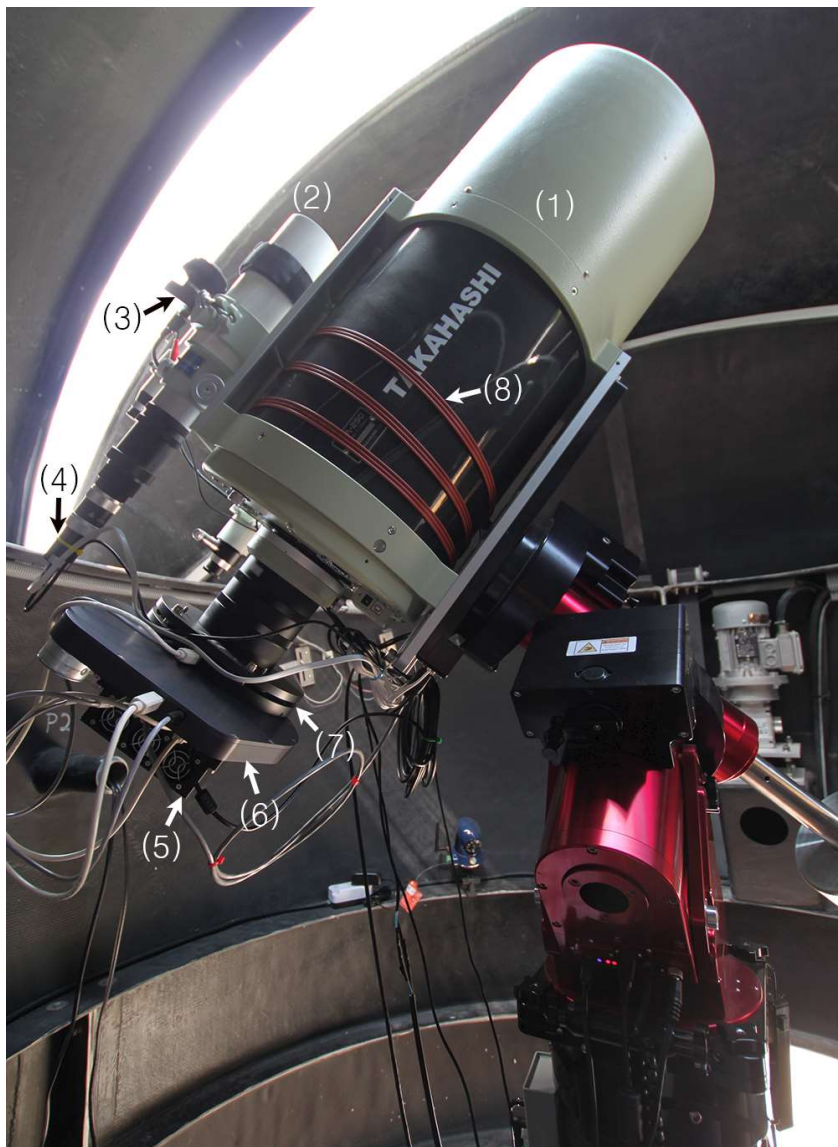


Figure 6. CCA-250 telescope system in MURO. (1) OTA(Optical Tube Assembly), (2) Guide scope, (3) Wide-field video camera, (4) Guide camera, (5) Science camera, (6) 7-position filter wheel, (7) Focuser, (8) Additional heating band that surround the primary mirror part of the tube.

Table 2

Characteristics of the CCA-250

Optical system	Corrected Cassegrain
Primary mirror diameter	250mm
Secondary mirror diameter	125mm
Focal length	1250mm
Focal ratio	f/5
Central obstruction	0.58
Optimal Field of View	88mm Image Circle

In Table 3, we tabulate the overall characteristics of the CCD sensor, and the science camera performance. The quantum efficiency(QE) of the CCD chip in the room temperature taken the information given by the Finger Lakes Instrumentation, Inc., 60% QE at 550nm wavelength. The currently available filters for CCD are two sets that combined 7-position filter wheel. First set is $UBVR_{\text{c}}$ of Johnson - Cousin photometric filters and H_{α} , $OIII$ of narrow-band filters. Secondary set is $LRGB$ of imaging filters and H_{α} , SII , $OIII$ of narrow band filters. All narrow band filters(H_{α} , SII , $OIII$) has 5.0nm bandwidth. These filters are 50mm square size with the thickness varying 3mm. The QE of CCD and Johnson - Cousins photometric filters passbands are shown in Figure 7. We also show list the effective wavelengths and the filter widths in FWHM in Table 4. The filters mounted on the two of each 7-position filter wheel manufactured by Finger Lakes Instrumentation, Inc. This is a single layer, 7-position filter wheel with a set of 7 filters placed on a circular table, which rotates when a filter change is needed. Each filter sets cannot be used simultaneously, there now the first filter set(photometric and H_{α} , $OIII$ narrow-band filters) is mounted. So it must be replaced manually for using an imaging filter set. The filter wheel can be controlled through USB communication line using a command line on Hyper - Terminal in Windows. Maxim DL can control science camera, guide camera, filter wheel, also data reduction. Generally, science images taken by Maxim DL and Data reduction can possible to AstroImageJ(AIJ).

Table 3

Sensor specifications of the FLI PL 16803 and performance

Sensor	Truesense KAF-16803
Pixels	4096×4096
Pixel Size	$9\mu\text{m}$
Pixel Scale	$1.485''/\text{pixel}$
Sensor Size	$36.8 \times 36.8\text{mm}$
Field of View	$1.69^\circ \times 1.69^\circ$
Sensor Diagonal	52mm
Full Well Capacity	100000 e ⁻
Typical Maximum Cooling	55°C below ambient
Typical Dark Current	$< 0.005\text{e}^-/\text{pixel}/\text{sec}$ at -35°C
Temperature Stability	0.1°C
Digitization Speed	1MHz, 8MHz
Typical System Noise	10e^- at 1MHz / 14e^- at 8MHz
Non-Linearity	$< 1\%$

These data of specifications measured by manufacturer, Finger Lakes Instrumentation, Inc.

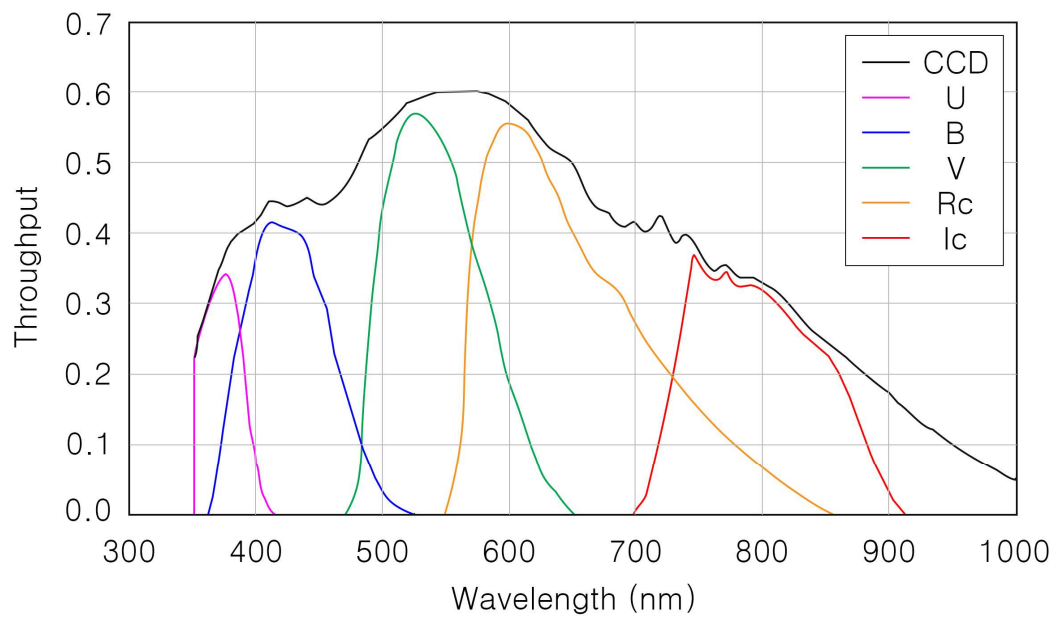


Figure 7. The QE of Truesense KAF-16803 sensor and Johnson - Cousin photometric filters passband.

Table 4

Filter wavelengths and widths

Photometric and narrow-band filters		
Filter name	λ_{eff} (nm)	$\Delta\lambda$ (nm)
U	366.3	65.0
B	436.1	89.0
V	544.8	84.0
R	640.7	158.0
I	798.0	154.0
H_{α}	656.3	5.0
$OIII$	500.7	5.0
Imaging filters		
Filter name	λ_{eff} (nm)	$\Delta\lambda$ (nm)
L	388.5 – 712.8	324.3
R	617.9 – 694.2	76.3
G	489.3 – 566.7	77.4
B	388.5 – 512.4	123.9
H_{α}	656.3	5.0
SII	671.6	5.0
$OIII$	500.7	5.0

These data of specifications measured by manufacturer, Optical Structures, Inc.

3. Data Reduction

Data taking can be done remotely whenever an observation is required. Focusing can be done with Maxim DL auto-focus process using the target or a with bright stars near the target. The typical auto-focus process takes 3 ~ 4 minutes, including the mount up slew time. Observing of the target is possible with Maxim DL and data reduction was performed with AstroImageJ(AIJ). When observing a target, each bias and dark frames taken in real time, and photometric filters are controlled by Maxim DL to take a flat field frames. Normally, the bias and dark frames are taken before performed the science image, and the flat field frames are taken regularly during twilight time with open the dome. In addition, bias and dark frames can be taken with close the cover of the telescope and the dome closed. AIJ provides an astronomy specific image display environment and tools for astronomy specific image calibration and data reduction. It is freeware and can run in WINDOWS or LINUX or Mac OS environments. Although AIJ maintains the general purpose image processing capabilities of ImageJ, AIJ is streamlined for time-series differential photometry, light curve detrending and fitting, and light curve plotting, especially for applications requiring ultra-precise light curves(e.g., exoplanet transits). It reads and writes standard FITS files, as well as other common image formats, provides FITS header viewing and editing, and World Coordinate System(WCS) aware, including an automated interface to the astrometry.net web portal for plate solving images. Although AIJ provides research grade image calibration and analysis tools, its GUI driven approach and cross-platform compatibility enable new users, even at the level of undergraduate student, high school student, teachers or amateur astronomer, to quickly start processing, modeling, and plotting astronomical image data with one tightly integrated software package(KAREN et al. 2016). AIJ data processor(DP) module automatically creates a master file and corrects the

image by specifying a folder and file name for bias, dark, and flat field frames taken with Maxim DL (show Figure 8). Each science image taken with Maxim DL can be automatically plate solving with reference to the FITS Header of the science image linked with astrometry.net according to the SIMBAD object ID⁴). Whenever a science image taken with Maxim DL is updated in a specified folder, AIJ will correct the science image and perform photometry according to the specified settings – bias and dark subtraction and flat fielding with a standard set of the AIJ’s calibration master files. Of course, this process can also be done with science images already taken, it can take all the science images and do data reduction later.

4) <http://simbad.u-strasbg.fr/simbad>

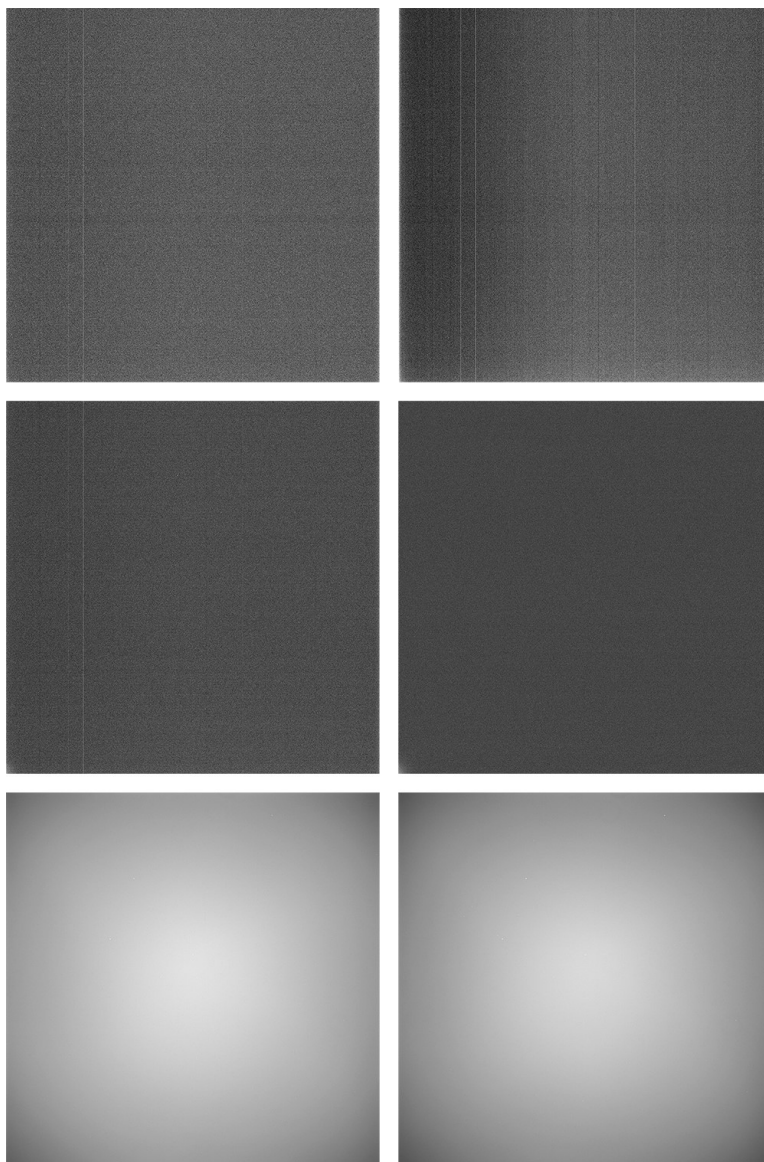


Figure 8. The bias, dark, and flat field frames taken with Maxim DL. In upper panel, shows the bias frames, and middle panel, shows dark frames. Left image is taken 1 frame and right image is master frame taken 20 frame combined with the 8MHz readout mode. Under panel, shows master flat field with 10 frame combined. Left image is B filter, and right image is V filter.

4. Standardization Results

4.1. Standard Star Observation

We perform absolute photometry by differential photometry function of AIJ with Landolt equatorial standard stars. We determine a target in 3h ~ 5h of right ascension where it is near the meridian during the observation period, November 2016. So we select the SA-95 in Landolt equatorial standard stars(Landolt, 2009), and we take the frame and doing flux calibration of twenty stars for the SA-95. Standard stars of this region were observed in dark clear nights of seeing condition of FWHM ~3.2 arcsec. Object images were bias and dark subtracted and flat fielded using data processor of AIJ. The instrumental magnitude was calculated by differential photometry function of AIJ with the BVRI filter for each stars. Instrumental magnitude can be transformed into the standard magnitude by the following equations:

$$B_i - B = zp_B + c_B(B - V) \quad (1)$$

$$V_i - V = zp_V + c_V(V - R) \quad (2)$$

$$R_i - R = zp_R + c_R(R - I) \quad (3)$$

$$I_i - I = zp_I + c_I(R - I) \quad (4)$$

In these equations, B_i , V_i , R_i , I_i are instrumental magnitudes by MURO, and zp_B , zp_V , zp_R , zp_I indicate zero point of each filters. Also, c_B , c_V , c_R , c_I are color coefficient, and capital letter B , V , R , I stands for the standard magnitude by Landolt. $(B - B_i)$ is a linear function on color index $(B - V)$, so we determine c and zp by finding y-intercept and slope of this function for standard stars(show Figure 9). The slope of function indicate coefficients c , and the value of y-intercept indicate zp . We carry out photometric weighted fitting algorithm to improve accuracy from the reduced chi-squared method:

$$\chi^2 = \frac{1}{k-1} \sum_i^k \frac{(O_i - C_i)^2}{\sigma_i^2} \quad (5)$$

In equation (5), where k is the number of target stars, O is the observed data and C is calculated data. σ indicates the photometric error in observed data. The coefficients were derived by the least square fitting algorithm with sigma clipping method($3\text{-}\sigma$). The photometric weighted fitting algorithm proceeds to ensure that the χ^2 has a minimum value. Table 5 shows the coefficient of *BVRI* filters with variation error.

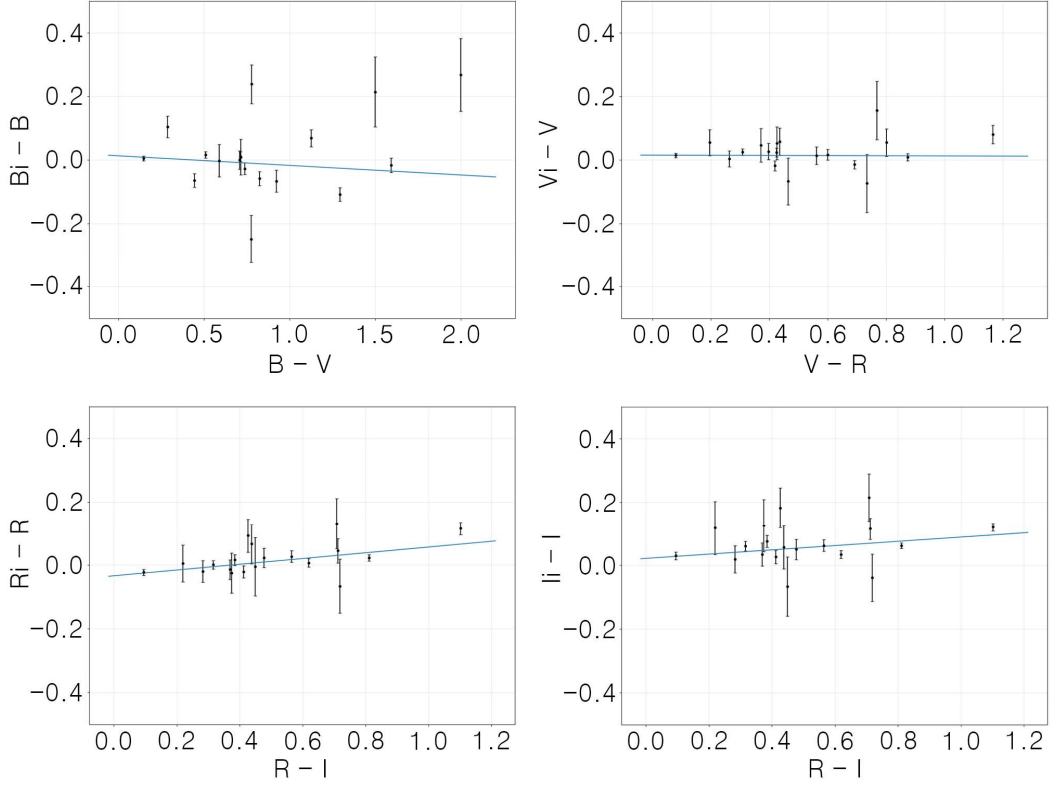


Figure 9. Slope of function for BVRI filters. It was calculated function from method of least squares. The slope of function indicate color coefficients (c) of each filters, and the value of y-intercept indicate zero point (zp). By photometric weighted fitting algorithm, the actual error is smaller than the error bar range of the each graph.

Table 5

Photometric calibration parameters from standard star data

Filter	$zp \pm zp_{err}$	$c \pm c_{err}$	M_{err}
B	0.013 ± 0.008	-0.030 ± 0.012	0.128
V	0.015 ± 0.007	-0.003 ± 0.013	0.050
R	-0.034 ± 0.008	0.090 ± 0.015	0.043
I	0.022 ± 0.010	0.067 ± 0.015	0.065

These coefficients were derived by fitting algorithm with sigma clipping method($3\text{-}\sigma$).

4.2. NGC 869 / 884 Observation

To test the on-sky performance of MURO, we observed open clusters NGC 869 / 884 field. We detected 183 stars in the NGC 869, and 106 stars in the NGC 884. The observed region of NGC 869 / 884 is shown in Figure 10. They were taken on the same night with standard stars observed, so seeing condition of FWHM is ~ 3.2 arcsec. The stars included in the field area was selected by referring to the SIMBAD, and we removed field stars that do not belong to the cluster using color - magnitude and color - color correlations to get only star cluster members. Then we have to conduct the photometric calibration for *BVRI* filters. Since the color index(e.g. $B - V$) is a standard magnitude, we need to convert the equations (1)–(4) to an expression for the absolute magnitude by MURO. So we combine the equations (1)–(4) for each filters to the matrix equations:

$$\begin{aligned} \begin{pmatrix} B_i \\ V_i \\ R_i \\ I_i \end{pmatrix} &= \begin{pmatrix} zp_B \\ zp_V \\ zp_R \\ zp_I \end{pmatrix} + \begin{pmatrix} B \\ V \\ R \\ I \end{pmatrix} + \begin{pmatrix} c_B \\ c_V \\ c_R \\ c_I \end{pmatrix} \left[\begin{pmatrix} B \\ V \\ R \\ I \end{pmatrix} - \begin{pmatrix} V \\ R \\ I \\ I \end{pmatrix} \right] \\ &= \begin{pmatrix} zp_B \\ zp_V \\ zp_R \\ zp_I \end{pmatrix} + \begin{pmatrix} 1+c_B & -c_B & 0 & 0 \\ 0 & 1+c_V & -c_V & 0 \\ 0 & 0 & 1+c_R & -c_R \\ 0 & 0 & c_I & 1-c_I \end{pmatrix} \begin{pmatrix} B \\ V \\ R \\ I \end{pmatrix} \end{aligned}$$

So, the converted absolute magnitude by MURO given:

$$B = \frac{B_i - zp_B - c_B V}{1 + c_B} \quad (6)$$

$$V = \frac{V_i - zp_V + c_V R}{1 + c_V} \quad (7)$$

$$R = \frac{R_i - zp_R + c_R I}{1 + c_R} \quad (8)$$

$$I = \frac{I_i - zp_I - c_I R}{1 - c_I} \quad (9)$$

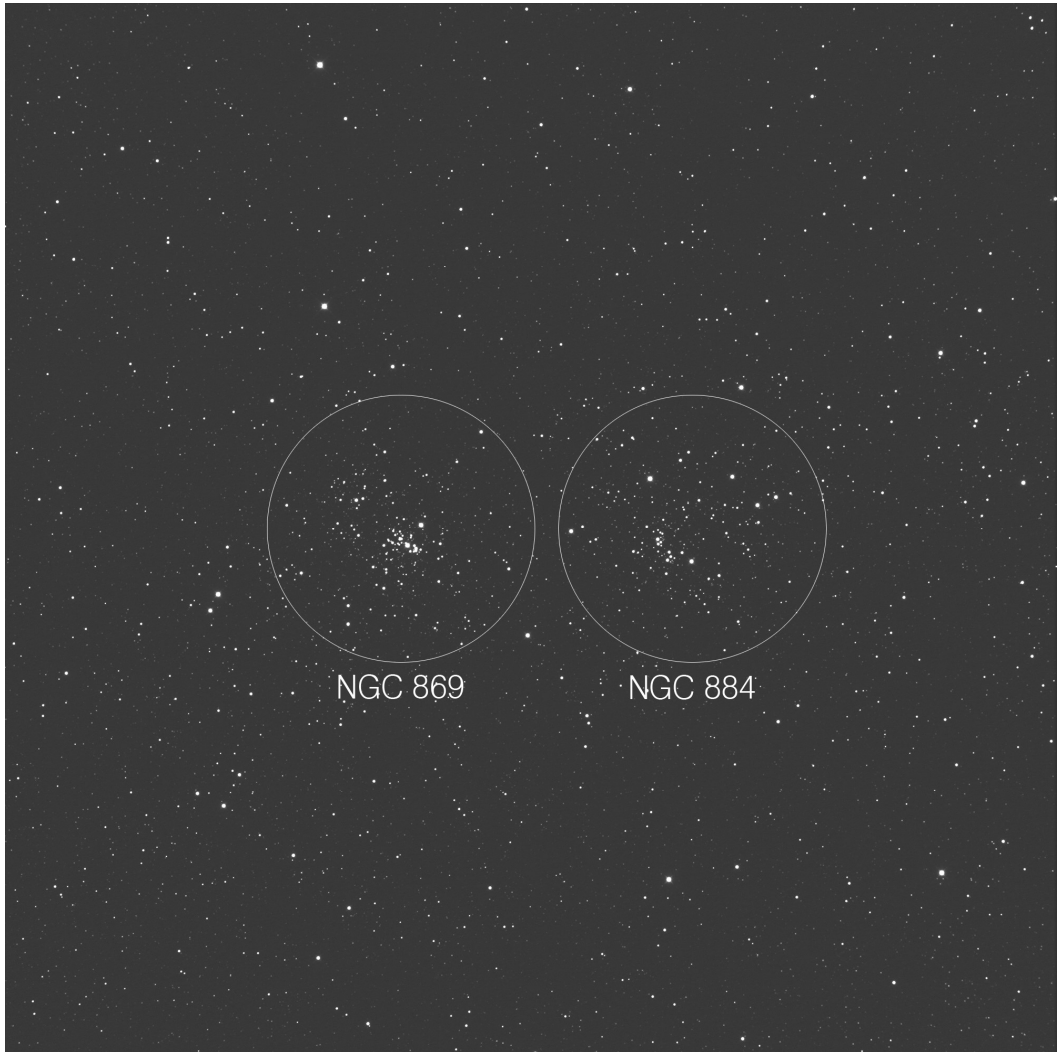


Figure 10. Photometric target region of NGC 869 / 884 open clusters in $1.69^\circ \times 1.69^\circ$ field of view(FOV) from MURO. The white circle boundary on the left points to NGC 869, and the right to NGC 884. We detected 289 point source stars in this region.

Now we can apply the equations (6)–(9) to find the absolute magnitude of the $BVRI$ observed with MURO. We already derived color coefficient (c) for each filter, in Section 4.1. So it can determine the zero point (zp) more precisely because the color coefficient (c) does not vary unless the instrumentation changes, and the number of fitting parameter is reduced. The zero point and limiting magnitude from NGC 869 / 884 open clusters is given in Table 6, and also plotted in Figure 11. The limiting magnitudes prefer the exposure time of 120 sec and the $10\text{-}\sigma$ detection of a point source. After identifying the same stars in B and V filters images, we compared magnitude B with color index ($B-V$) correlations for individual stars to derived MURO data and SIMBAD. The Figure 12 shows the color – magnitude diagram result of comparing MURO and SIMBAD for NGC 869 / 884. This color – magnitude diagrams from the observed MURO values follow the similar form as the diagrams from the SIMBAD. The similarity of result for the photometric calibration parameters shows that it can be applied not only to this target(NGC 869 / 884) but also to other objects or clusters.

Table 6

Photometric calibration parameters from NGC 869 / 884 data

Filter	$zp \pm zp_{err}$	M_{err}	Limiting Magnitude
B	0.039 ± 0.014	0.122	18.308
V	-0.093 ± 0.005	0.060	18.547
R	0.347 ± 0.024	0.117	19.096
I	-0.362 ± 0.025	0.121	16.887

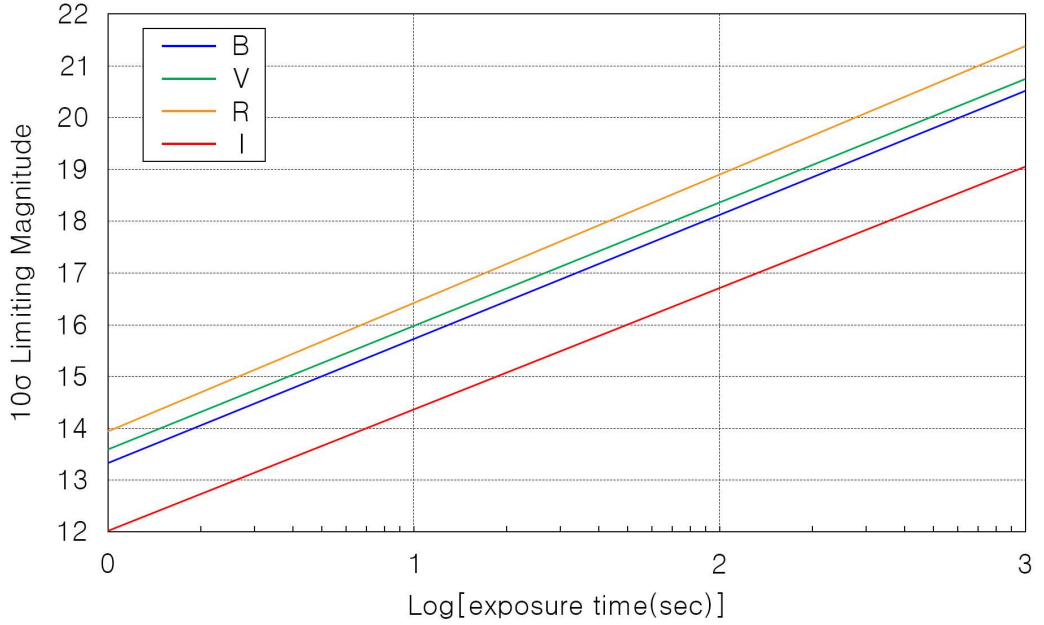


Figure 11. The limiting magnitudes of MURO as a function of exposure time from the NGC 869 / 884 field. The blue, green, orange, red lines show the respectively results for the B, V, R, I filters.

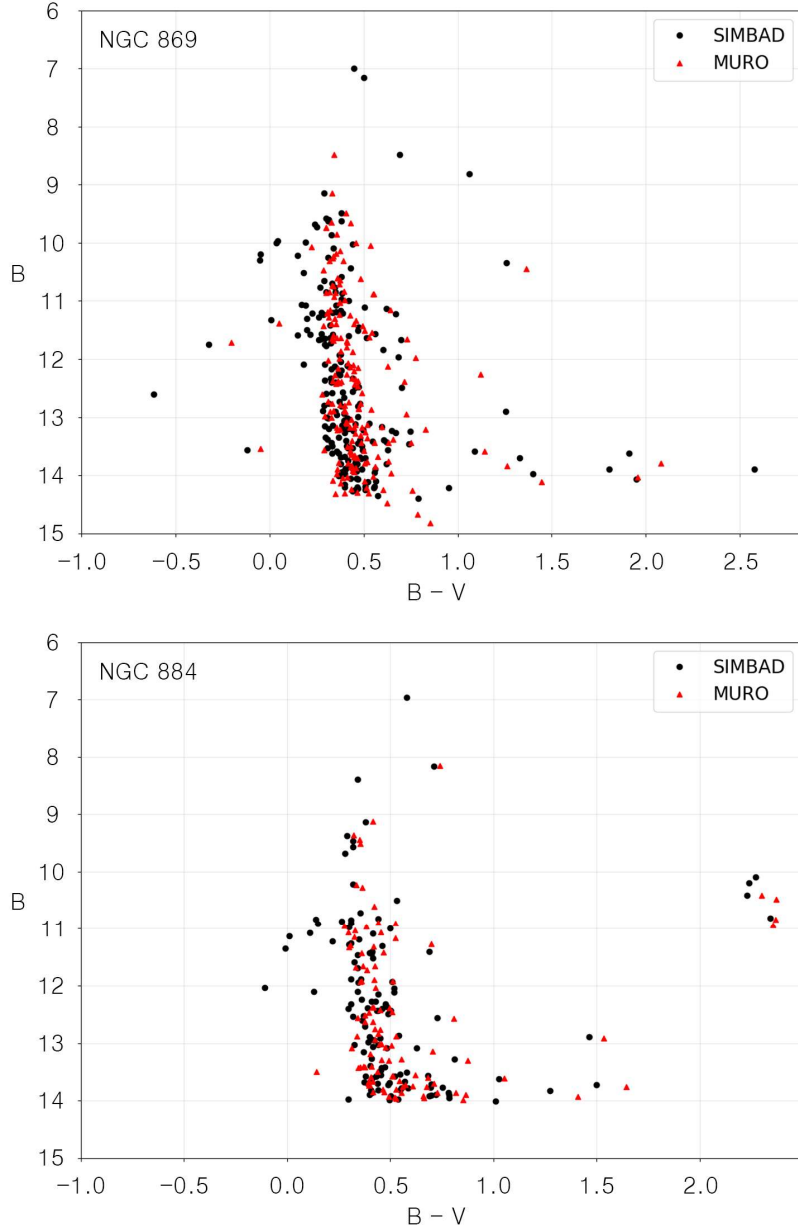


Figure 12. The color - magnitude diagram result of comparing SIMBAD(black filled circles) and MURO(red filled triangles) for NGC 869 / 884. In upper panel shows the NGC 869, and under panel shows NGC 884.

5. Summary

We have presented the characteristics and the performance of the MURO system that is installed on Yangpyeong in KOREA. The remote 0.25 m telescope(CCA-250) with a pixel scale of 1.485 arcsec($9\mu\text{m}$) in $4\text{K} \times 4\text{K}$ CCD camera provides $1.69^\circ \times 1.69^\circ$ wide field of view(FOV). This is equipped with the $UBVR_cI_c$ of Johnson-Cousin photometric filters, H_α , $S\Pi$, $O\Pi\text{I}$ of narrow band filters(5.0nm bandwidth) and $LRGB$ imaging filters. It provides a good images that the limiting magnitude of $B = 18.308\text{mag}$, $V = 18.547\text{mag}$, $R = 19.096\text{mag}$, $I = 16.887\text{mag}$ at $10\text{-}\sigma$ with 120 sec exposure time. We are convinced that applying the coefficients calculated here makes photometry of various stars and clusters very easy and fast. Also, we confirmed that our observation facility can be used for serious astronomical research ranging from variable star monitoring, supernovae follow-up observation, and narrow band imaging survey as well as simple research for educational purpose of amateurs and students or teachers with permission from Mangpo high school astro-laboratory. If MURO is further stabilized in the future, it could be used for citizen astronomy projects for more researchers.

< References >

- Barrado-Izagirre, N., Rojas, J. F., Hueso, et al. 2013, Jupiter's Zonal Winds and Their Variability Studied with Small-Size Telescopes, *A&A*, 554, A74
- Bessell, M. S. 2005, Standard Photometric Systems, *ARSS*, 43, 293
- Brown, T. M., Baliber, N., et al. 2013, Las Cumbres Observatory Global Telescope Network, *PASP*, 125, 1031
- Bumbungan, M. T., Priyatikanto, R. P. et al. 2019, Two 0.5-m Robotic Telescopes for Timau National Observatory in Eastern Indonesia, *IOP*, 1231, 012008
- Choi, C., & Im, M. 2017, Seoul National University Camera II (SNUCAM-II): The New SED Camera for the Lee Sang Gak Telescope (LSGT), *JKAS*, 50, 71
- Collins, K. A., Kielkopf, J. F. et al. 2017, AstroImageJ: Image Processing and Photometric Extraction for Ultra-Precise Astronomical Light Curves, *ApJ*, 153, 77
- French J. et al., 2004, Gamma-Ray Bursts: 30 Years of Discovery, 727, 741
- Gebhardt, P., Schrimpf, A., et al. 2019, U - SmART: Small Aperture Robotic Telescopes for Universities, *RMxAA*, 51, 44
- Gillon, M., Jehin, E. et al. 2011, TRAPPIST: a robotic telescope dedicated to the study of planetary systems, *EDPS*, 11, 06002
- Gorbovskoy, E. S., Lipunov, V. M. et al. 2013, The MASTER-II Network of Robotic Optical Telescopes, *Astronomy Reports*, 57, 233
- Grauer, A. D., Neely, A. W., & Lacy, C. H. S. 2008, Building an Automated Telescope with High Photometric Accuracy, *PASP*, 120, 992
- Gupta, R., Singh, H. P., Kanbur, S. M., Schrimpf, A., & Dersch, C. 2015,

- U-SmART – Small Aperture Robotic Telescopes for Universities, PKAS, 30, 683
- Hardy, L. K., Butterley, T., Dhillon, V. S. et al. 2015, pt5m – a0.5m Robotic Telescope on La Palma, MNRAS, 454, 4316
- Hodapp, K. W. 2014, Infrared Imaging and Spectroscopy with Small Telescopes. CAOSP, 43, 200
- Im, M., Ko, J. et al. 2010, Seoul National University 4K \times 4K Camera (SNUCAM) for Maidanak Observatory, JKAS, 43, 75
- Im, M., Choi, C., & Kim, K. 2015, Lee Sang Gak telescope (LSGT): a remotely operated robotic telescope for education and research at Seoul National University, JKAS, 48, 207
- Kanbach, G., Rau, A., & Slowikowska, A. 2014, Fast Photometry with Small Telescopes, CAOSP, 43, 216
- Katysheva, N., Zharova, A., & Shugarov, S. 2014, The Investigation of Nova M31 2005 – 13 with Small Telescopes, CAOSP, 43, 447
- Keller, S. C., Grebel, E. K. et al. 2001, UBVI and H_α Photometry of the Persei Cluster, ApJ, 122, 248
- Kim, E., Kim, Y. et al. 2015, Detection of an Impact Flash Candidate on the Moon with an Educational Telescope System, JASS, 32, 121
- Kim, E., Park, W.-K., Jeong, H., et al. 2011, Auto-Guiding System for CQUEAN (Camera for QUasars in EARly uNiverse), JKAS, 44, 115
- Kim, K. M., Son, D. H. et al. 1997, Determination of Atmospheric Extinction Coefficient at Bohyunsan Optical Astronomy Observatory, PKAS, 12, 167
- Kim, S., Jeon, Y. et al. 2016, Development of SED Camera for Quasars in Early Universe (SQUEAN), PASP, 128, 115004
- Klotz, A., Boer, M., Eysseric, J. et al. 2008, Robotic Observations of the sky with TAROT: 2004 – 2007, PASP, 120, 1298

- Landolt, A. U. 2009, UBVRI Photometric Standard Stars Around The Celestial Equator: Updates and Additions, *ApJ*, 137, 4186
- Lim, J., Chang, S., Pak, S. et al. 2013, Focal Reducer for CQUEAN (Camera for QUasars in EArly uNiverse), *JKAS*, 46, 161
- Marshall, P. J., Lintott, C. J., & Fletcher, L. N. 2015, Ideas for Citizen Science in Astronomy, *ARAA*, 53, 247
- McCrady, N., Nava, C. et al. 2014, Minerva Exoplanet Detection Sensitivity from Simulated Observations, *AAS*, 223, 34803
- Paczynski, B. 2006, Astronomy with Small Telescopes, *PASP*, 118, 1621
- Park, W. K., Pak, S., Im, M., et al. 2012, Camera for QUasars in EArly uNiverse(CQUEAN), *PASP*, 124, 839
- Park, W., Pak, S. et al. 2016, Photometric Transformation from RGB Bayer Filter System to Johnson - Cousins BVR Filter System, *ASR*, 57, 509
- Pedani, M. 2009, Sky Surface Brightness at Mount Graham: UBVRI Science Observations with the Large Binocular Telescope, *PASP*, 121, 778
- Schmitt, J. H. M. M., Schroder, K. P. et al. 2014, TIGRE: A new robotic spectroscopy telescope at Guanajuato, Mexico, *AN*, 335, 787
- Snellen, I. A., Stuik, R. et al. 2012, Ground-Based Search for the Brightest Transiting Planets with the Multi-Site All-Sky CAmERA: MASCARA, *SPIE*, 8444,84440I
- Steele, I. A., Smith, R. J. et al. 2004, The Liverpool Telescope: performance and first results, *SPIE*, 5489, 679
- Strolger, L. G., Gott, A. M. et al. 2014, The RCT 1.3m robotic telescope: broadband color transformation and extinction calibration. *ApJ*, 147, 49
- Tarady, V., Sergeev, O. et al. 2014, Studies of NEOs as a Task for Small Telescopes, *CAOSP*, 43, 434

- Topasna, G. A., Topasna, D. M., & Popko, G. B. 2013, An Easily Designed and Constructed Optical Polarimeter for Small Telescopes, *PASP*, 125, 1056
- Tsapras, Y., Street, R. et al. 2009, RoboNet-II: Follow-up observations of microlensing events with a robotic network of telescopes. *Astronomische Nachrichten*, AN, 330, 4-11
- Wittenmyer, R. A., Johnson, J. A. et al. 2015, MINERVA: Small Planets from Small Telescopes. *PKAS*, 30, 665
- Zerbi R. M. et al. 2001, The REM telescope: detecting the near infra red counterparts of Gamma Ray Bursts and the prompt behavior of their optical continuum, *AN*, 322, 275